Analyst

PAPER

View Article Online
View Journal | View Issue

Cite this: *Analyst*, 2015, **140**, 243

In vitro HER2 protein-induced affinity dissociation of carbon nanotube-wrapped anti-HER2 aptamers for HER2 protein detection†

Javed H. Niazi,*[a] Sandeep K. Verma,[a] Sarfaraj Niazi[b] and Anjum Qureshi[a]

A new *in vitro* assay was developed to detect human epidermal growth factor receptor 2 (HER2) protein, based on affinity dissociation of carbon nanotube (CNT)-wrapped anti-HER2 ssDNA aptamers. First, we selected an anti-HER2 ssDNA aptamer (H2) using an *in vitro* serial evolution of ligands by an exponential enrichment (SELEX) process. Then the fluorescently labelled H2 ssDNAs were tightly packed on CNTs that had previously been coupled with magnetic microbeads (MBs), forming MB–CNT–H2 hybrids. The loading capacity of these MB–CNTs heterostructures (2.8×10^8) was determined to be 0.025 to 3.125 μM of H2. HER2 protein-induced H2 dissociation occurred from MB–CNT–H2 hybrids, which was specifically induced by the target HER2 protein, with a dissociation constant (K_d) of 270 nM. The stoichiometric affinity dissociation ratio with respect to H2-to-HER2 protein was shown to be approximately 1 : 1. Our results demonstrated that the developed assay can be an effective approach in detecting native forms of disease biomarkers in free solutions or in biological samples, for accurate diagnosis.

Received 10th September 2014
Accepted 16th October 2014

DOI: 10.1039/c4an01665c

www.rsc.org/analyst

1. Introduction

Nanomaterials are now used in a wide spectrum of applications in the biomedical field. They have been effectively utilized to deliver biologically active cargo to the sites of interest for purposes of cancer diagnosis and therapy.[1–3] Various nanostructured materials such as carbon nanotubes (CNTs),[4] polymeric nanoconjugates,[5,6] and nanoparticles[7,8] have been explored, especially in cancer therapy.[9] The unique physicochemical properties of CNTs have been exploited as popular tools in cancer diagnosis and therapy.[10] They are considered one of the most promising nanomaterials, with the capability of both detecting cancerous cells and delivering small therapeutic molecules.[10] In addition, CNTs can effectively shuttle various bio-molecules into cells, including drugs,[3,11] peptides,[12] proteins,[13] plasmid DNA,[14] small interfering RNA,[15] and aptamers,[16] *via* endocytosis.[17] Therefore, it is imperative to develop new methods utilizing the unique physicochemical properties of CNTs in biomedical applications, including the detection of cancer biomarkers at the early stages with high specificity and selectivity.

Tumor-targeted therapies require ligands that can bind to cancer cells where aptamers can represent an alternative therapeutic modality. These molecules are small, single-stranded DNA or RNA in nature.[18] Aptamers have great prospects in therapeutic applications, especially in cancer treatment. For example, AS1411, a nucleolin-specific truncated version of an aptamer called GRO29A, is currently in advanced clinical trials.[19] Other therapeutic aptamers that have been tested for antiviral, anticoagulation, anti-inflammatory and anti-angiogenic properties are already in clinical trials.[20] Macugen is the first clinically approved aptamer made of ssRNA molecules that effectively inhibits macular degeneration.[21] With the aim of creating a more effective tool for cancer diagnosis, we considered human epidermal growth factor receptor 2 (HER2) as a target cancer marker protein.

HER2, also known as ErbB2, Neu, CD340 or P185 is a transmembrane tyrosine kinase receptor and a member of the epidermal growth factor receptor (EGFR or ErbB) family. Overexpression of ~20–30% HER2 is shown to be associated with aggressive breast cancer cases.[22] The overexpression of HER2 levels is also linked to other cancers, including ovarian, lung, gastric, and oral.[22,23] Therefore, it is imperative to monitor HER2 levels to enable early cancer diagnosis. Existing methods for detecting HER2 are based on expensive biopsies followed by conducting immunohistochemistry (IHC) and fluorescence *in situ* hybridization (FISH) techniques for detecting HER2 protein levels.[24,25] Synthetic tyrosine kinase inhibitors such as erlotinib

[a]*Sabanci University Nanotechnology Research and Application Center, Orta Mah, 34956 Istanbul, Turkey. E-mail: javed@sabanciuniv.edu; Fax: +90 216 483 9885; Tel: +90 216 483 9879*

[b]*Department of Pharmaceutical Chemistry, JSS College of Pharmacy, SS Nagara 570015, Mysore, Karnataka, India*

† Electronic supplementary information (ESI) available: Fig. S1 illustrating the SELEX process, FTIR spectra of MB-CNTs and MB-CNTs-ssDNAs (Fig. S2), and list of aptamer variants (sequences) evolved to bind against HER2 protein after the SELEX process. See DOI: 10.1039/c4an01665c

and gefitinib as well as monoclonal antibodies, such as cetuximab and trastuzumab, have been developed to inhibit pathological signaling or to recruit the immune system against cancer cells.[26,27]

Targeting HER2 with low molecular weight kinase inhibitors has established this family of receptors as an effective target for novel drugs. Thus, therapeutic use of anti-HER2 aptamers is a promising alternative to monoclonal antibodies and kinase inhibitors for clinical applications, mainly because of their relatively low production cost as well as low batch-to-batch variability.[27] Anti-HER2 aptamers have been increasingly developed that have high affinity and specificity to HER2, and these have been shown to inhibit proliferation of cultured cancer cells.[28–32] Nevertheless, there is still a need for developing new aptamer variants against cancer biomarkers that can potentially serve as inhibitory agents for cancer diseases. Determination of increased HER2 protein levels in human serum is an alternative approach of utilizing such aptamers in combination with CNT structures so as to enable the treatment of cancer in its early stages and the effective prevention of traumatic events.

In this paper, we first hypothesize an *in vitro* delivery system which utilizes CNTs that carry anti-HER2 aptamers and release specifically when the target HER2 protein is supplied in the synthetic medium. This hypothesis was experimentally tested by first selecting a specific anti-HER2 aptamer using the SELEX process. The selected anti-HER2 aptamer was packed around CNTs by physical wrappings that had in turn been previously coupled with MBs. These heterogeneous structures were employed to demonstrate the specific dissociation of anti-HER2 aptamers, which was induced by their strong affinity toward HER2 protein. This feature is most desirable for a ligand molecule to qualify for potential targeted drug-delivery application under *in vivo* conditions.

2. Experimental

2.1 *In vitro* selection of ssDNA aptamers that bind HER2

2.1.1 Preparation of HER2 protein-coated magnetic beads. Pure and carrier-free recombinant HER2 (ErbB2) protein (R&D Systems®) was first conjugated with surface-activated magnetic Dynabeads® M-270 Carboxylic Acid (Invitrogen, USA) using a carbodiimide coupling method as described by the manufacturer. The HER2 protein-coated beads were magnetically separated and washed thrice with 100 μL of PBS, pH 8 containing 0.05% Tween 80 and finally resuspended in 100 μL of PBS, pH 7.4 containing 0.1% BSA and stored at 4 °C. Thus obtained, the HER2 protein-coated beads were utilized for *in vitro* selection of ssDNA aptamers using the SELEX process.

2.1.2 Negative selection. Negative selection was carried out as a prerequisite step to eliminate the non-specific oligos from the initial random ssDNA pool prior to beginning the anti-HER2 aptamer selection process. For this, $\sim 10^{15}$ diverse ssDNAs molecules (random library) with the sequence 5′-GGGCCGTTCGAACACGAGCATG$(N)_{40}$GGACAGTACTCAGGTCATCCTAGG-3' (pool-1) were incubated with each aliquot of $\sim 2 \times 10^7$ beads coated with (i) ethanolamine and (ii) BSA, followed by (iii) naked beads, to eliminate the non-binders from the main ssDNA pool. The residual ssDNA pool (pool-2) was resuspended in 1 : 10 diluted human serum (male; blood type, AB+; PANTM Biotech GmbH) in 1× binding buffer (100 mM NaCl, 20 mM Tris–HCl pH 7.6, 2 mM $MgCl_2$, 5 mM KCl, 1 mM $CaCl_2$, 0.02% Tween 20) allowing removal of undesirable oligos, and this mixture containing random, free ssDNA pool (pool 3) was finally utilized for the SELEX process.

2.1.3 SELEX. It was essential to subject the random ssDNA pool to thermal treatment in order to attain their most stable confirmations before allowing these molecules to be incubated with the target protein. Therefore, at the beginning of each selection round, the initial ssDNAs were denatured at 90 °C for 10 min and quickly cooled at 4 °C for 15 min followed by incubation for 7 min at room temperature (25 °C). The pretreated ssDNA pool was later utilized for selection of anti-HER2 aptamers using SELEX, as per the method described previously.[33] Details of the steps involved in the SELEX process are schematically shown in (ESI) Fig. S1.†

The HER2 protein-bound sequences were eluted, purified and amplified by symmetric/asymmetric PCR using the forward primer, 5′-fluorescein-GGGCCGTTCGAACACGAGCATG-3′ (F1) and the reverse primer, 5′-GGACAGTACTCAGGTCATCCTAGG-3′ (R1). Amplified PCR product (dsDNA) carrying the aptamer sequence was labelled fluorescently during the PCR reaction, and was extracted after resolving on 2% agarose gel followed by purification using a gel extraction kit (QIAquick, Qiagen). Purified dsDNA was further resolved by denaturation polyacrylamide gel electrophoresis (PAGE, 12%), using 7 M urea containing 20% formamide, and isolation of the target fluorescent ssDNAs by gel excision followed by extraction using a PAGE gel extraction kit (Qiaex II). Obtained ssDNAs were measured using a Nanodrop spectrophotometer (Thermo Scientific) and applied as the isolated ssDNA fraction in the next selection round, as the starting pool. The above process was repeated for at least 12 cycles of selection, each comprising a series of steps as illustrated in Fig. S1.† An optimized PCR program was used to amplify the HER2-bound ssDNAs as follows: initial 15 min denaturation at 95 °C, 35–40 cycles of 30 s denaturation at 94 °C, 30 s annealing at 53 °C and 30 s amplification at 72 °C, respectively, with a final extension step at 72 °C for 10 min. The final pool of selected aptamers was cloned using a TOPO-TA cloning kit (Invitrogen) and sequenced. The secondary structure prediction of the aptamer sequences was evaluated using m-fold web server (utilizes free energy minimizing algorithm) available at http://www.bioinfo.rpi.edu/applications/mfold.[34] As a result, 7 positive clones designated as H1–H7 were obtained, from which one of the aptamers, H2, was selected for further studies. All experimental methods related to the cloning and screening of positive clones are described in the ESI section.†

2.2 *In vitro* assay for affinity displacement/dissociation of anti-HER2 aptamers

2.2.1 Fabrication of MB–CNTs heterostructures and binding assays. Magnetic microbeads (Dynabeads®, M270

Amine, MBs) were covalently coupled with carboxyl-functionalized multi-walled CNTs O.D. × L = 10–20 nm × 5–30 μm (Arry®, Hong Kong). Stock CNTs (1 mg mL^{-1}) were dispersed in 0.1% Tween 20, and the suspension was homogenized by ultrasonication using a probe sonicator (Bandelin, Germany), and a well-dispersed and homogeneous CNT suspension was added to the magnetic beads with intermittent agitation to allow physical interaction of CNTs with the magnetic beads, according to the method previously described.[35] The thus-formed magnetic microbeads coated with uniform layers of CNTs were isolated by applying an external magnetic field. The magnetic nature of MBs allowed extensive washing of MB–CNTs for the effective removal of unattached CNTs and thereby minimized the surfactant effect. After extensive washing, the inherent brown color of MBs turned black, indicating the strong attachment of CNTs on the surface.[35] SEM images were taken of the beads for further confirmation of the homogeneous CNT layer coating. To prevent attachment of surface CNTs present on MB–CNTs, the MB–CNTs were suspended in a mild surfactant solution (0.01% Tween 20), which facilitated the homogeneous suspension of MB–CNTs. The thus-formed MB–CNT heterostructures were utilized for further studies.

2.2.2 Physical adsorption of anti-HER2 ssDNAs on MB–CNTs heterostructures. A constant amount (2.8 × 10^8) of MB–CNT heterostructures was incubated with varying ssDNA concentrations in 1× binding buffer (BB). Here, the ssDNAs used were 5′ labelled with fluorescein in order to trace the fluorescence levels (emission at 523 nm) in the reaction mixture after excitation at 470 nm. The reaction mixture was incubated on a vortex mixer for 15 min at room temperature. The binding capacity of MB–CNTs with ssDNAs was estimated by measuring the fluorescence (λ_{523}) in the supernatant solution using a Nanodrop Fluorospectrometer (Nanodrop Technologies, Inc., USA). The MB–CNT–ssDNA hybrids were washed in a series of steps until the supernatant showed no detectable fluorescence and finally stored at 4 °C until use. The physical wrapping of ssDNAs around CNTs was confirmed by Fourier transform infrared spectroscopy (FTIR; Nicolet 6700). The ssDNA loading capacity of MB–CNT heterostructures was calculated to be a maximum of 3.125 μM ssDNA with 2.8 × 10^8 MB–CNTs. Stability tests of MB–CNT–ssDNA hybrid structure were carried out and the detailed steps are described in the ESI section.†

2.2.3 HER2 protein-dependent affinity dissociation of anti-HER2 aptamers from MB–CNT–ssDNA hybrid structures. Ten identical aliquots, each carrying 4 × 10^7 MB–CNT–ssDNA hybrid structures were suspended in 200 μL 1× BB. These aliquots were divided into two pools, each with 5 aliquots, for test and control groups. A constant 10 μL of 300 nM of HER2 protein prepared from stock 7.5 μg/200 μL in 1× BB was added and incubated for binding against a series of different concentrations of ssDNA wrapped on MB–CNTs (MB–CNT–ssDNA hybrids). The binding kinetics and HER2 protein-induced ssDNA dissociation by unwinding from hybrid structures (affinity separation) were studied. The beads were magnetically separated and the fluorescence was measured in the supernatant, which corresponded to the amount of ssDNAs dissociated from MB–CNT–ssDNA hybrids. For controls, instead of HER2 protein, BSA was used as a non-specific protein. The above process was repeated until reaching a saturation point.

2.2.4 Kinetics of anti-HER2 aptamer (MB–CNT–ssDNAs hybrids) interaction with HER2 protein and dissociation constant (K_d). First, a standard plot of known concentrations of fluorescein-labelled H2 ssDNA *versus* fluorescence emission at 523 nm was established. A series of controlled numbers of MB–CNT–ssDNA heterostructures corresponding to 0.025–3.125 μM H2 ssDNAs was incubated with a constant 300 nM HER2 protein in 1× BB solution for 15 min. For respective controls, BSA was used as a non-specific protein. Relative fluorescence units (RFUs) directly obtained by fluorospectrometer (which, according to the manufacturer, is derived from the relationship between 2–4 wavelengths) was measured from the aqueous phase and the values converted to H2 ssDNA concentration (affinity dissociated) and plotted against the initial ssDNA concentrations added. The data points were fitted using non-linear regression analysis, and the dissociation constant was calculated with the help of the SigmaPlot v12 program using one-site saturation, under ligand-binding mode, which utilized the following equation:

$$y = B_{max} \times \text{free ssDNA}/K_d + \text{free ssDNA} \quad (1)$$

where y is degree of saturation, B_{max} is the number of maximum binding sites (here one-site binding option was employed), and K_d is the dissociation constant.[36]

3. Results and discussion

3.1 *In vitro* selection of anti-HER2 aptamers

Anti-HER2 aptamers were selected *in vitro* through directed selection by combinatorial screening of random library of ~10^{15} ssDNA using the SELEX technique. As a result, seven aptamer candidates were evolved that bound to HER2 protein in a complex human serum medium. The sequences of the seven selected aptamers (H1–H7) are listed in Table S1.† The binding preference of an aptamer is important for its application as a targeting ligand. An ideal tumor-targeting aptamer should bind to the target molecule with minimal binding to other proteins. Here, we found that the H2 sequence evolved multiple times within the window of <50–60 nucleotides from the SELEX process compared with the other aptamer candidates, indicating its strong preference towards binding to HER2 protein. Since albumin is the most abundant protein in blood, we spiked HER2 protein in 1 : 10 diluted human serum as a background component for *in vitro* selection and binding studies. The anti-HER2 aptamer (H2) chosen in this study also had a most stable confirmation due to its double strandedness, because of its more negative ΔG value, after H1, from among the seven aptamer candidates.[34] The calculated ΔG with the following H2 sequence—5′-GGGCCGTCGAACACGAGCATGGTGCGTGGACCT AGGATGACCTGAGTACTGTCC-3′ (M.W. = 16.72 kDa)—was −6.69 kcal mole^{-1}. This result indicated that the single strandedness of the aptamer was able to spontaneously transform into its most stable double stranded structure (Fig. 1). The predicted

secondary structure of H2 showed two stem-loops and the random sequence was found to be located in its major stem-loop structure, which was predicted to be the binding site for HER2 protein (Fig. 1).

3.2 *In vitro* affinity dissociation of anti-HER2 aptamers

A new assay scheme was designed for testing *in vitro* HER2-induced displacement or delivery of the anti-HER2 aptamer (H2), in order to determine its stoichiometric binding or release with respect to the H2-to-HER2 protein ratio. Interaction of DNA and CNTs facilitates formation of supramolecular complexes[37] and such interactions have been shown to adhere tightly, and to form a uniform and stable film that has been exploited for useful applications.[38] Here, CNTs were employed as cargos (matrix) for carrying H2 ssDNAs that were coated on MBs so as to form heterostructures for testing HER2 target protein-induced displacement (affinity dissociation) in the medium (Scheme 1).

A heterogenous matrix made of CNTs decorated on MBs was confirmed by SEM examination. Fig. 2a and b shows SEM images of MBs before and after uniform layer coating with CNTs. A small increase in the size of dynabeads was observed after coating with CNTs, as seen in Fig. 2b. The H2 ssDNAs were then allowed to tightly pack by physical wrapping on CNTs as described in the Experimental section. Binding of fluorescein-labelled H2 on MB–CNTs was examined by measuring the fluorescence intensity at 523 nm that showed diminishing fluorescence in the reaction supernatant as a result of strong H2–CNT interactions compared with the control. The diminishing of fluorescence can be attributed to strong physical wrapping of ssDNAs on CNTs present on MBs. Further, wrapping of ssDNAs on CNT structures was confirmed by FTIR spectra (Fig. S2†). The extent of H2 adsorption or loading capacity with 2.8×10^8 MB–CNTs was determined to be in the range 0.025–3.125 μM H2 until reaching a saturation point (Fig. 2c–f).

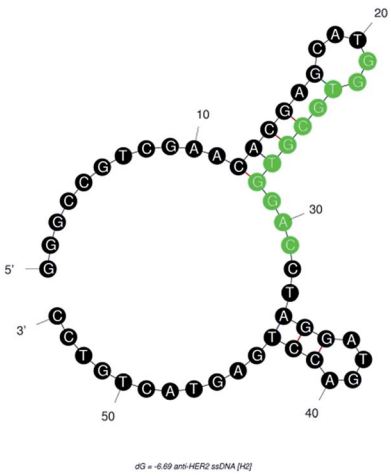

Fig. 1 Secondary structure of anti-HER2 (H2) aptamer predicted using a free-energy minimizing algorithm, m-fold web server. The highlighted random region is predicted to be the HER2 protein-binding sequence.

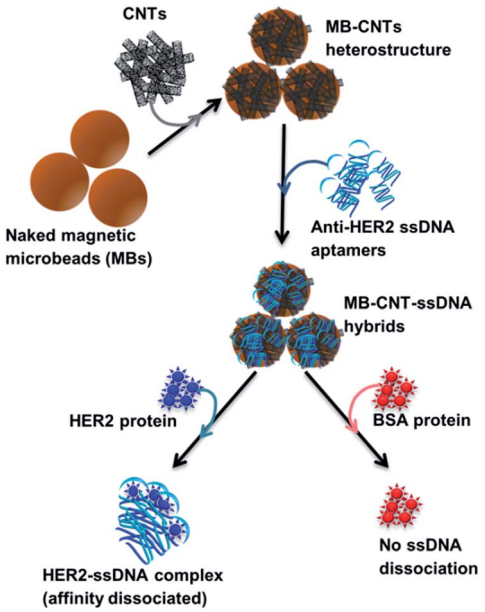

Scheme 1 Schematic diagram showing sequential steps involved in *in vitro* method employed for HER2-specific targeted release/dissociation of H2 from MB–CNT–H2 cargos. Note that the graphics of beads, ssDNA or proteins shown in the scheme do not reflect their actual size or dimensions.

3.3 Stability of MB–CNT–H2 hybrid structures

MB–CNT–H2 hybrid structures were subjected to stability tests by thermal and chemical denaturation. The released fluorescence intensities at 523 nm were measured for dissociation of CNT-wrapped ssDNAs at varying temperatures from 4 to 94 °C for 1 h. Fluorescence emission profiles of H2 released from MB–CNT–ssDNA hybrids against varying temperatures with time showed that no significant unwrapping of ssDNAs occured from CNT–ssDNAs hybrid structures at temperatures 4–94 °C (ESI,† Fig. 3). However, a partial dissociation of ssDNAs from hybrid structures did occur but only with 0.1% SDS, probably due to surfactant-induced unfolding or unwrapping of ssDNAs. It is clear from the above results that the ssDNAs were tightly wrapped on MB–CNTs, which required a strong surfactive agent such as SDS to dissociate them from CNTs.

3.4 *In vitro* HER2 protein-induced affinity release of H2 from MB–CNT–H2 (cargos)

Competitive stoichiometric dissociation of H2 ssDNAs was initially postulated to occur by the influence of HER2 protein in the reaction mixture as schematically illustrated in Scheme 1. This hypothesis was tested by allowing interaction of HER2 protein with MB–CNT–ssDNA hybrid structures (cargos). Dissociation because of the strong binding affinity of H2 toward HER2 protein was therefore determined using a series of MB–CNT–ssDNA hybrid structures ($1–5 \times 10^7$) loaded with 0.05–0.3 μM H2 ssDNAs. These hybrid structures were incubated with a

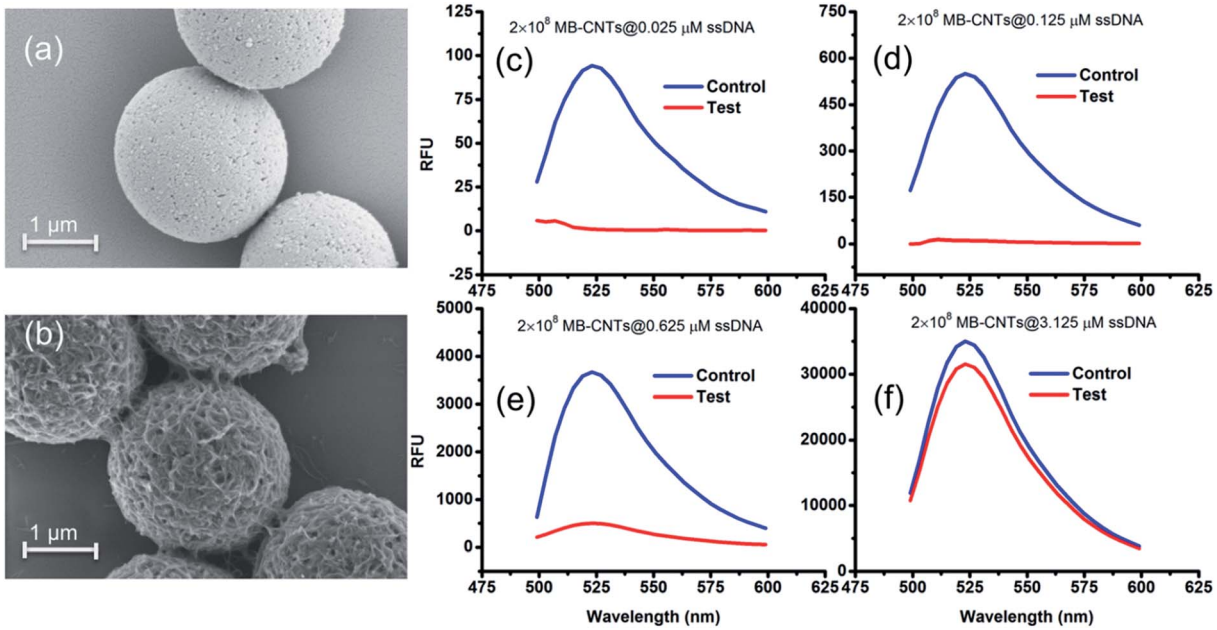

Fig. 2 SEM images of (a) bare MBs and (b) fabricated MB–CNT heterostructures. The MB–CNTs (2×10^8) were loaded with fluorescein-labelled H2 ssDNA at different concentrations, such as (c) 0.025 μM, (d) 0.125 μM, (e) 0.625 μM, and (f) 3.125 μM, and the released fluorescence (after excitation at 470 nm) in the reaction supernatant before (blue) and after incubation (red) with MB–CNTs are shown in (c) to (f).

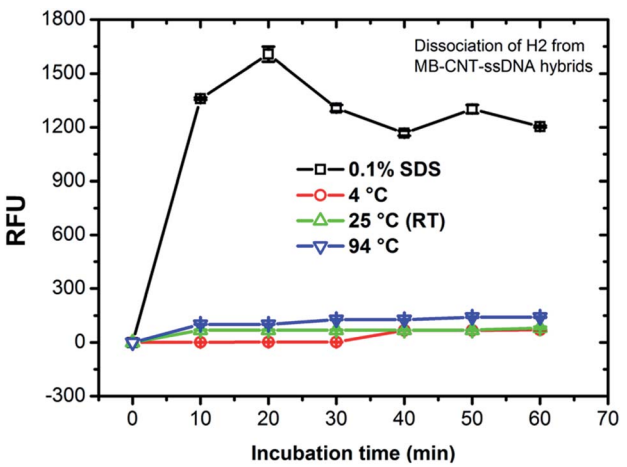

Fig. 3 Stability of MB–CNT–H2 hybrid structure suspended in binding buffer (BB) after thermal and surfactant treatments. Relative fluorescence units (RFUs) measured after the MB–CNT–ssDNAs suspension incubated for 1 h at different temperatures on a surfactant, as shown in the legend. The figure shows that non-specific dissociation of H2 in the aqueous phase of the reaction mixture occured only with 0.1% SDS.

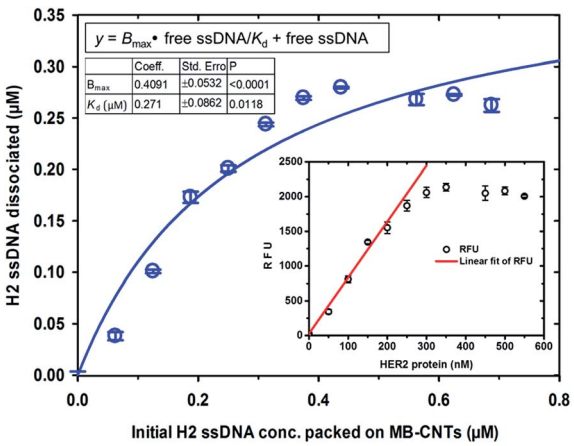

Fig. 4 Binding of HER2 protein with increasing concentrations of free ssDNA (H2) aptamers that were affinity-dissociated from the tightly packed MB–CNT–ssDNA hybrid structures. Saturation curve was obtained after plotting the concentration of affinity-dissociated H2 ssDNA against constant HER2 protein (300 nM). The inset shows a linear fit of measured RFU values, corresponding to the linear range of HER2 protein concentrations.

constant 300 nM pure and carrier-free form of HER2 protein. HER2 protein-induced dissociation of H2 was evidenced from MB–CNT–ssDNA hybrids, which was dose-dependent and accompanied by an increase in fluorescence intensity (Fig. 4). The reaction supernatant contained the H2 ssDNA–HER2 protein complex; this exhibited a fluorescence property because of the fluorescein dye at its 5′-end that did not quench, as opposed to that seen with QD-conjugated H2 in dot-blot assays. As the number of MB–CNT–ssDNA conjugates increased, H2 binding with HER2 increased as well, until reaching a saturation point (Fig. 4).

The H2 ssDNA corresponding to the RFU values were fitted using non-linear regression analysis, and the dissociation constant (K_d) according to one-site binding was calculated to be 270 nM with 300 nM HER2 protein present in the reaction mixture. This result indicated that an approximate 1 : 1 stoichiometric molecular binding occurred with ssDNA-to-HER2

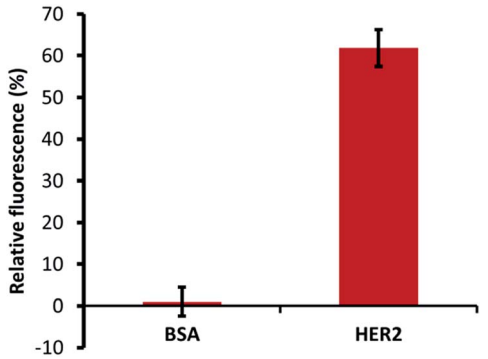

Fig. 5 Affinity dissociation of H2 from constant MB–CNT–H2 hybrid structures incubated with the same amount of BSA and HER2 proteins (300 nM). The H2 aptamer was dissociated only in the presence of HER2 protein, but not in the presence of BSA, a non-specific protein.

protein. Similar 1 : 1 stoichiometric binding with EGF and EGFR was reported by another research group.[39] Further, a dynamic detection range of 50–250 nM was established using the measured RFU values corresponding to HER2 protein that exhibited a limit of detection of 38 nM (47.5 ng/10 μL sample volume) of HER2 protein (Fig. 4). This range is comparable to previously reported studies.[40]

The specific ability of H2 binding with HER2 protein was confirmed by specificity tests using a constant number of MB–CNT–ssDNAs incubated against each protein (HER2/BSA) at equimolar concentrations that showed no non-specific displacement of H2 occurred against BSA protein (Fig. 5). The methods employed in this study therefore hold an advantage of H2 ssDNA binding with HER2 protein in its native and free forms, which is most desirable in clinical diagnosis, thus making the developed assay a simple and rapid tool for specific and accurate biomarker detection.

4. Conclusions

The present study provides a unique strategy to target HER2 protein for the detection of protein biomarkers in the context of cancer diagnosis or therapy using anti-HER2 aptamers. HER2 is overexpressed in many tumors, providing binding sites that can be directly accessible to aptamers from circulating blood. The high affinity and specificity of aptamers with HER2 protein from tumor cells are useful targets for the sensitive and accurate diagnosis of various types of cancers. In this study, H2 anti-HER2 aptamer was selected *in vitro* and employed on the basis of its ability to effectively bind to HER2 protein in the complex human serum environment. This method did not require any additional chemical reagents, enabling detection of HER2 protein in its native forms in human serum and thus making it a highly preferred method in clinical diagnosis.

Use of CNTs for targeted delivery is a significant development in the field of therapeutic nanomedicine or cancer diagnosis for targeting cells that abundantly express HER2 protein. The strategy of target-induced affinity dissociation is a promising alternative to existing technologies for cancer diagnosis or therapy. Therefore, a unique *in vitro* method was developed aimed at testing MB–CNTs as cargos of H2 ssDNAs. These cargos were loaded with calculated amounts of fluorescently labelled anti-HER2 aptamer (H2) and successfully tested for its ability for programmable release, which was influenced by the presence of abundant HER2 protein in the medium. This strategy can potentially be explored in *in vivo* models for anti-HER2 aptamers as inhibitory drug-delivery systems. Our study demonstrated that the aptamer-mediated cancer diagnosis could be explored further as anti-HER2 therapy or detection of HER2 levels in serum.

Acknowledgements

This work was supported by the Scientific and Technological Research Council of Turkey (TUBITAK; grant no. 110E287) for JHN. We thank Ashish Pandey, Irena Roci, and Lisa Elif Archibald for their assistance with SEM analysis, aptamer selection, and binding assays, respectively.

Notes and references

1 Y. Fukumori and H. Ichikawa, *Adv. Powder Technol.*, 2006, **17**, 1–28.
2 J. K. Vasir and V. Labhasetwar, *Adv. Drug Delivery Rev.*, 2007, **59**, 718–728.
3 A. H. Faraji and P. Wipf, *Bioorg. Med. Chem.*, 2009, **17**, 2950–2962.
4 M. Prato, K. Kostarelos and A. Bianco, *Acc. Chem. Res.*, 2007, **41**, 60–68.
5 S. R. Mane, V. Rao, N. K. Chaterjee, H. Dinda, S. Nag, A. Kishore, J. Das Sarma and R. Shunmugam, *Macromolecules*, 2012, **45**, 8037–8042.
6 H. Zhou, W. Yu, X. Guo, X. Liu, N. Li, Y. Zhang and X. Ma, *Biomacromolecules*, 2010, **11**, 3480–3486.
7 A. G. Tkachenko, H. Xie, D. Coleman, W. Glomm, J. Ryan, M. F. Anderson, S. Franzen and D. L. Feldheim, *J. Am. Chem. Soc.*, 2003, **125**, 4700–4701.
8 J. Song, J. Zhou and H. Duan, *J. Am. Chem. Soc.*, 2012, **134**, 13458–13469.
9 C. Wang, C. Wu, X. Zhou, T. Han, X. Xin, J. Wu, J. Zhang and S. Guo, *Sci. Rep.*, 2013, **3**, 2852.
10 S.-R. Ji, C. Liu, B. Zhang, F. Yang, J. Xu, J. Long, C. Jin, D.-L. Fu, Q.-X. Ni and X.-J. Yu, *Biochim. Biophys. Acta, Rev. Cancer*, 2010, **1806**, 29–35.
11 R. P. Feazell, N. Nakayama-Ratchford, H. Dai and S. J. Lippard, *J. Am. Chem. Soc.*, 2007, **129**, 8438–8439.
12 D. Pantarotto, J.-P. Briand, M. Prato and A. Bianco, *Chem. Commun.*, 2004, 16–17.
13 N. W. S. Kam and H. Dai, *J. Am. Chem. Soc.*, 2005, **127**, 6021–6026.
14 Y. Liu, D. C. Wu, W. D. Zhang, X. Jiang, C. B. He, T. S. Chung, S. H. Goh and K. W. Leong, *Angew. Chem.*, 2005, **117**, 4860–4863.
15 N. W. S. Kam, Z. Liu and H. Dai, *J. Am. Chem. Soc.*, 2005, **127**, 12492–12493.

16 S. M. Taghdisi, P. Lavaee, M. Ramezani and K. Abnous, *Eur. J. Pharm. Biopharm.*, 2011, **77**, 200–206.
17 N. W. S. Kam, Z. Liu and H. Dai, *Angew. Chem.*, 2006, **118**, 591–595.
18 R. Stoltenburg, C. Reinemann and B. Strehlitz, *Biomol. Eng.*, 2007, **24**, 381–403.
19 E. M. Reyes-Reyes, Y. Teng and P. J. Bates, *Cancer Res.*, 2010, **70**, 8617–8629.
20 K.-T. Guo, G. Ziemer, A. Paul and H. P. Wendel, *Int. J. Mol. Sci.*, 2008, **9**, 668–678.
21 E. W. Ng, D. T. Shima, P. Calias, E. T. Cunningham Jr, D. R. Guyer and A. P. Adamis, *Nat. Rev. Drug Discovery*, 2006, **5**, 123–132.
22 D. J. Slamon, W. Godolphin, L. A. Jones, J. A. Holt, S. G. Wong, D. E. Keith, W. J. Levin, S. G. Stuart, J. Udove and A. Ullrich, *Science*, 1989, **244**, 707–712.
23 M.-C. Hung, A. Matin, Y. Zhang, X. Xing, F. Sorgi, L. Huang and D. Yu, *Gene*, 1995, **159**, 65–71.
24 M. Milburn, M. Rosman, W. C. Mylander, W. Liang, J. Hooke and A. Kovatich, *Ann. Surg. Oncol.*, 2011, **18**, S176.
25 M. Arnedos, A. Nerurkar, P. Osin, R. A'Hern, I. E. Smith and M. Dowsett, *Ann. Oncol.*, 2009, **20**, 1948–1952.
26 F. Ciardiello and G. Tortora, *N. Engl. J. Med.*, 2008, **358**, 1160–1174.
27 G. Mahlknecht, R. Maron, M. Mancini, B. Schechter, M. Sela and Y. Yarden, *Proc. Natl. Acad. Sci. U. S. A.*, 2013, **110**, 8170–8175.
28 G. C. Shao, J. Wang, Z. H. Li, L. Saraf, W. J. Wang and Y. H. Lin, *Sens. Actuators, B*, 2011, **159**, 44–50.
29 K. Dastjerdi, G. H. Tabar, H. Dehghani and A. Haghparast, *Biotechnol. Appl. Biochem.*, 2011, **58**, 226–230.
30 C. L. Esposito, D. Passaro, I. Longobardo, G. Condorelli, P. Marotta, A. Affuso, V. de Franciscis and L. Cerchia, *PloS One*, 2011, **6**, e24071.
31 M. Y. Kim and S. Jeong, *Nucleic Acid Ther.*, 2011, **21**, 173–178.
32 B. C. Chi-hong, G. A. Chernis, V. Q. Hoang and R. Landgraf, *Proc. Natl. Acad. Sci. U. S. A.*, 2003, **100**, 9226–9231.
33 R. Stoltenburg, C. Reinemann and B. Strehlitz, *Anal. Bioanal. Chem.*, 2005, **383**, 83–91.
34 M. Zuker, *Nucleic Acids Res.*, 2003, **31**, 3406–3415.
35 H. Ünal and J. H. Niazi, *J. Mater. Chem. B*, 2013, **1**, 1894–1902.
36 M. Müller, J. E. Weigand, O. Weichenrieder and B. Suess, *Nucleic Acids Res.*, 2006, **34**, 2607–2617.
37 M. Zheng, A. Jagota, E. D. Semke, B. A. Diner, R. S. Mclean, S. R. Lustig, R. E. Richardson and N. G. Tassi, *Nat. Mater.*, 2003, **2**, 338–342.
38 C. G. Hu, Y. Y. Zhang, G. Bao, Y. L. Zhang, M. L. Liu and Z. L. Wang, *J. Phys. Chem. B*, 2005, **109**, 20072–20076.
39 P. J. Brennan, T. Kumogai, A. Berezov, R. Murali and M. I. Greene, *Oncogene*, 2000, **19**, 6093–6101.
40 J. T. Gohring, P. S. Dale and X. D. Fan, *Sens. Actuators, B*, 2010, **146**, 226–230.